ORIGINAL ARTICLE

Enhancement of Heat Transfer in a Cavity Containing a Periodically Moving Flexible Fin: Application of NEPCM

Nehila Tarek[1] (iD) | Mohammad Ghalambaz[2,3] (iD) | Muneer Ismael[4,5] (iD) | Mikhail Sheremet[6] | Benachour Elhadj[1]

[1]ENERGARID Laboratory, Tahri Mohamed University of Bechar, Bechar, Algeria | [2]Department of Mathematical Sciences, Saveetha School of Engineering, SIMATS, Chennai, India | [3]Refrigeration and Air conditioning Technical Engineering Department, College of Technical Engineering, The Islamic University, Najaf, Iraq | [4]Mechanical Engineering Department, Engineering College, University of Basrah, Basra, Iraq | [5]College of Engineering, University of Warith Al-Anbiyaa, Karbala, Iraq | [6]Laboratory on Convective Heat and Mass Transfer, Tomsk State University, Tomsk, Russia

Correspondence: Nehila Tarek (Nehila.tarek@univ-bechar.dz)

ABSTRACT

This study investigates the enhancement of natural convection heat transfer in a differentially heated square cavity by coupling fluid–structure interaction (FSI) with a nanofluid containing nanoencapsulated phase change material (NEPCM). This configuration is important for improving passive cooling in energy-efficient technologies, such as electronics, buildings, and electric vehicles. The novelty of this study lies in the integration of a sinusoidal oscillating flexible fin with latent-heat-enhanced nanofluids in a fully coupled FSI framework. A finite element method is used to solve the governing equations for fluid flow, heat transfer, and structural motion, with validation through grid independence tests and comparison against benchmark numerical and experimental data. Parametric studies were performed for fin oscillation amplitude (0.05–0.15), oscillation period (0.1–0.7), Rayleigh number (10^4–10^6), and Stefan number (0.2–0.7). Results show that increasing the amplitude to 0.15 enhances the mean Nusselt number by up to 10%; lower periods ($\tau_{fin} = 0.1$) and Stefan numbers ($Ste = 0.2$) reduce heat transfer; higher Rayleigh numbers promote stronger convective currents and better thermal uniformity. These findings offer quantitative insights for optimizing thermally responsive structures using NEPCM fluids and flexible fins, enabling efficient heat transfer.

1 | Introduction

The implementation of phase change material (PCM) technology emerged in the mid-20th century with advancements in scientific research in the energy sector. Initially, these materials were primarily applied in air conditioning systems and thermal solar panels (collectors). However, their adoption remained limited due to their low thermal conductivity, a crucial parameter in heat transfer processes.

To overcome this limitation, a new generation of materials, nanoencapsulated phase change materials (NEPCMs), was developed [1]. These materials feature PCM encapsulated within micro- or nanometric structures, which enhances their thermophysical performance by increasing the heat exchange surface area, thus optimizing heat transfer efficiency, and promoting their usage in cooling of central processing unit [2] and other electronics [3] applications.

In this study, we focus on the application of NEPCM in closed cavities subjected to differential heating. The review study of [4] emphasized many trends towards using this strategy in enhancing the storage of energy. However, to this end, we present below the most significant and recent works that have addressed this topic. Aissa et al. [5] investigated forced convection heat exchange in a complex triangular chamber. The study

analyzed the effect of varying the position of a rotating cylinder, revealing that the presence of the cylinder can enhance heat exchange by up to 240%. Abderrahmane et al. [6] examined a partially wavy cavity containing a flame-shaped heat source. The study evaluated the combined effects of wall dynamics, magnetic field, and porosity, demonstrating that an enhancement in magnetic field intensity and opposite movement of the lateral walls significantly reduce the convective heat transfer coefficient. Conversely, a decrease in the Hartmann number led to a Nu increase ranging from 11.5% to 640%. Abderrahmane et al. [7] studied a three-dimensional wavy trapezoidal cavity, finding that reducing the number of undulations on the lower wall improves heat transfer. Additionally, for Reynolds numbers between 1 and 100, a thermal enhancement of up to 51% was observed. Ghalambaz et al. [8] investigated thermal transport in a quadrangular circular enclosure filled with an NEPCM suspension. The study showed that at high Hartmann number values, heat exchange is reduced due to the Lorentz force's effect on fluid velocity. Optimal fusion temperature values ($\theta_f = 0.35$ and 0.675) were identified, and a higher concentration of nanoparticles led to improved heat transfer. Aljibori et al. [9] assessed heat exchange mechanisms and entropy generation in an NEPCM confined within a cavity altered by embedding wavy blocks on the upper and lower faces. Using optimal parameters ($\phi = 0.05$) resulted in a 12% increase in Nu and a 33% reduction in entropy generation. Hussain et al. [10] explored the bioconvective flow of an NEPCM in a rectotrapezoidal cavity, demonstrating that the average heat transfer decreases as the Hartmann, Rayleigh, and Peclet numbers increase. Hussain et al. [11] examined the magnetobioconvective flow of nanoenhanced PCM in an H-shaped cavity containing oxytactic microorganisms. The study showed that varying the cavity's aspect ratio (AR) enhances bioconvective flow and PCM behavior. Moreover, the thermal Rayleigh number and bioconvective Rayleigh number play key roles in improving heat transfer.

On the other hand, to control fluid flow within cavities and natural convection heat transfer, inserting solid bodies—whether stationary or in motion—has garnered significant interest among researchers across various fields. The primary objective is to study the interaction between solid structures and fluid flow. Below, we present key studies that have explored the effects of fins and membranes on fluid flow and their influence on energy transfer. The first study investigating the effect of a moving fin was conducted by Ghalambaz et al. [12] in a square chamber subjected to periodic motion. The results demonstrated that higher oscillation amplitudes of the fin lead to better heat transfer, with a dimensionless length of $L = 0.2$ found to be optimal for maximizing this exchange. A similar study by Alsabery et al. [13] in an oblique cavity analyzed various parameters, including the ratio of heat transfer rates, dimensionless elastic modulus, oscillation amplitude, left wall radiator length, and wall angle of tilt. The findings revealed that wall inclination significantly improves heat transfer. In the same context, a study by Shahabadi et al. [14] examined the coupled effect of a non-Newtonian fluid and an elastic fin, showing that the transition between pseudoplastic, Newtonian, and the dilatant effects causes a decline in heat transfer performance and an increase in the internal stresses in the fin. Furthermore, in Saleh et al. [15], the effect of two thin and

flexible fins was investigated, demonstrating maximum heat transfer enhancement when optimizing parameters, such as opening size and fin oscillation direction. A more recent study by Tarek et al. [16] explored the impact of complex (wavy) geometry on the interaction between a solid and a fluid domain. By integrating a geometric parameter AR into the governing equations of both the solid and fluid, the authors demonstrated that effective control of flow dynamics and thermal exchange in complex cavities is achievable. This study establishes the basis for new thermal engineering applications based on geometry optimization. In another study, Tarek et al. [17] examined the effect of the position of a localized heat source within a fin (base, center, or tip) on flow behavior and thermal transport. The findings revealed that heat transfer is minimized when the heat source is placed at the center of the fin. Several other studies have investigated membrane interactions with various fluids to control flow and convective heat transfer driven by natural forces. For instance, in [18], a study on a circular cavity subjected to differential heating analyzed the influence of the Prandtl number over a range of $Pr = 0.71–200$. Similarly, Mehryan et al. [19] investigated a trapezoidal enclosure, revealing that the thermal transfer in the square cavity is 15% higher than in the trapezoidal one. Recent research [20] focused on the effect of a vertically oscillating adiabatic bar on heat transfer in a porous medium.

In a study conducted by [21], the authors investigated the rectilinear oscillatory motion of two spherical particles along the line connecting their centers in an axisymmetric, incompressible flow at low Reynolds number. Their findings showed good agreement with the analytical solutions for the steady motion of two spherical particles, as well as with the known behavior of single-particle oscillations. A related study conducted by the same author [22] examines the axisymmetric rotation of two eccentric spheres immersed in an incompressible couple-stress fluid within a porous annular region. The study concludes that the dimensionless couple becomes increasingly significant, as permeability contributes to the enhancement of parameters, such as particle size, torque, fluid constraints, and separation distance. In the same context, the oscillatory behavior of a micropolar fluid driven by pressure through a hydrophobic cylindrical microannulus under the influence of electroosmotic flow was investigated by [23]. The results indicate that the amplitude of resistance to microrotation increases significantly with higher values of the slip and spin parameters. Others, through a numerical investigation conducted by [24], addressed the enhancement of heat transfer and the reduction of irreversibility. The study focused on the behavior of a hybrid nanofluid and the analysis of entropy generation in a partially annular chamber. The results show that the incorporation of anchor-shaped fins and the increase in their number significantly enhance thermal performance while reducing system irreversibility. The maximum entropy generation was digitally estimated, revealing an increase of approximately 49.35%. Another recent numerical study conducted by the same author [25] investigates entropy generation and hydrothermal performance under buoyancy effects induced by a floating hybrid nanofluid. Curved heated fins were added to the inner cylinder, and the results revealed that curved fins represent the most effective design for enhancing heat transfer. In particular, Case 4 demonstrated an improvement of 1.74% in

overall heat transfer with increasing nanoparticle concentration. In [26], the authors examine the hydrothermal behavior of buoyancy-driven, magnetized hybrid nanofluid flow consisting of multiwalled carbon nanotubes, Fe_3O_4, and water, circulating between two centrally positioned circular cylinders. The results indicate that flow velocity increases with higher Rayleigh numbers, whereas the presence of a magnetic field and elevated nanoparticle concentrations tend to reduce the velocity.

While previous works addressed either flexible fins in simple fluids, or NEPCM materials in static systems, there is a lack of research addressing the coupled behavior of a deformable structure interacting with an NEPCM fluid under thermal convection. This study fills this gap by exploring the combined impact of structure motion, latent heat storage, and convective dynamics within a confined square geometry. The square cavity, which can be easily switched to rectangular geometry, serves as a simplified yet realistic model for many practical applications (e.g., electronic enclosures, photovoltaic cells, microthermal systems). The present problem offers quantitative insights for optimizing thermally responsive structures using NEPCM fluids and flexible fins, enabling efficient heat transfer enhancement.

2 | Mathematical Formulation

2.1 | Statement of the Problem and Underlying Assumptions

The studied problem is illustrated in Figure 1. It involves a thermoconvective analysis in a square enclosure with side length L, incorporating thermal coupling with fluid–structure interaction (FSI). For more generalized analysis, the problem is treated in dimensionless form. The structural element under investigation is a thin fin with length of $a = 0.25$ and width of $b = 0.01$, positioned at the midpoint of the lower wall, that is, at $L/2$. The working fluid is a homogeneous suspension of nanostructured PCM-filled capsules, well dispersed in a base fluid. The objective is to analyze the impact of this innovative fluid on heat exchange and the naturally induced flow field characteristics inside the cavity.

The boundary conditions are defined by thermally contrasted sidewalls: the left wall is held at a cold temperature $T_c = 0$, whereas the right wall is subjected to a hot temperature $T_h = 1$. The upper and lower horizontal walls are thermally insulated. These thermal gradients induce a natural fluid motion, influenced by convective phenomena and FSI effects.

The governing equations of fluid–solid coupling (FSI) in both the solid (fin) and fluid domains, as well as those describing the phase change of NEPCMs, are well established in the literature [6, 12, 17, 27].

We use the following dimensionless parameters:

$$(u, v, w) = \frac{(u^\circ, v^\circ, w^\circ)L}{\alpha_f}, \quad P = \frac{L^2}{\rho_f \alpha_f{}^2}P^\circ, \quad T = \frac{\left(T^\circ - T_c^\circ\right)}{\left(T_h^\circ - T_c^\circ\right)},$$
(1)

$$d_{fin} = \frac{d_{fin}^\circ}{L}, \quad \sigma = \frac{\sigma^\circ}{E^\circ}, \quad t = \frac{t^\circ \alpha_f}{L^2}, \quad (x, y, a, b) = \frac{(x^\circ, y^\circ, a^\circ, b^\circ)}{L}.$$
(2)

2.2 | Solid Domain (Fin)

The equations describing the geometrically nonlinear elastodynamic behavior and the energy of the fin are given as follows [12]:
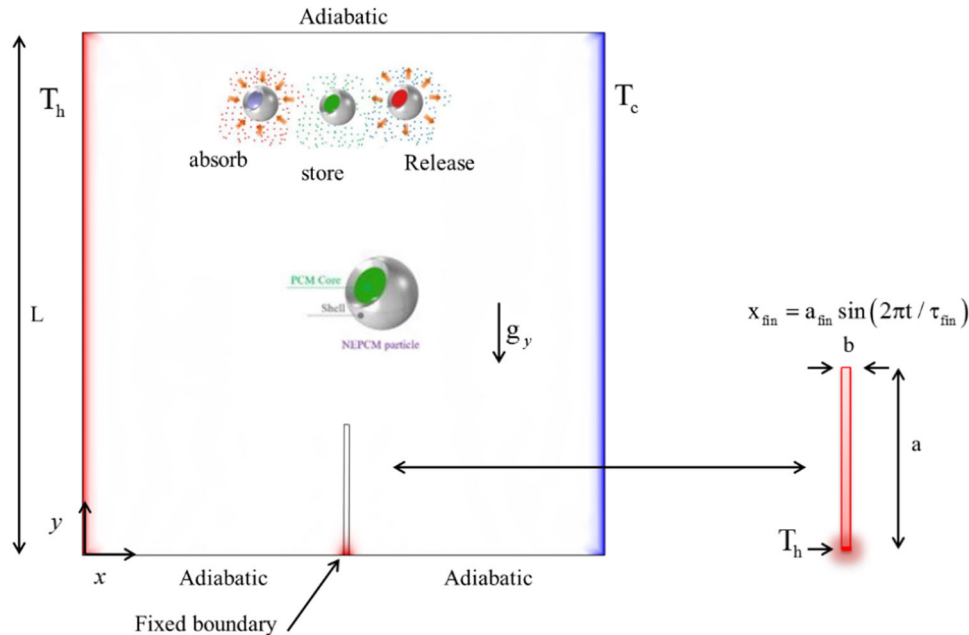

FIGURE 1 | A physical representation of an equilateral (square) enclosure with a periodically moving fin. [Color figure can be viewed at wileyonlinelibrary.com]

$$\frac{1}{\rho_r}\frac{d^2 d_{\text{fin}}}{dt^2} - E\nabla\sigma - EF_v = 0, \quad (3)$$

$$\frac{\partial T}{\partial t} - \alpha_r \nabla^2 T = 0, \quad (4)$$

where $E = E^o L^2/\rho_f \alpha_f^2$ is the flexibility parameter, and $F_v = (\rho_f - \rho_{\text{fin}})Lg_y/E^o$ is the body force, $\rho_r = \rho_f/\rho_{\text{fin}}$ and $\alpha_r = \alpha_{\text{fin}}/\alpha_f$ are, respectively, the density ratio and thermal diffusivity, the ratio parameter.

Assuming a linearly elastic behavior for the fin and incorporating geometric nonlinearity, the stress tensor is formulated as $\sigma = J^{-1}FSF^T$ with $F = \left(I + \nabla d_{\text{fin}}^o\right)$ and $J = \det.(F)$. The stress tensor in the second Piola–Kirchhoff formulation S [28] is connected to the strain ε as

$$S = C : (\varepsilon) \; with \; \varepsilon = 1/2\left(\nabla d_{\text{fin}}^o + \nabla d_{\text{fin}}^{oT} + \nabla d_{\text{fin}}^{oT}\nabla d_{\text{fin}}^o\right) \quad (5)$$
$$where \; C = C(E^o, v).$$

The following formula defines the dimensionless displacement at fin's tip:

$$x_{\text{fin}} = a_{\text{fin}}\sin(2\pi t/\tau_{\text{fin}}) \quad (6)$$

with a_{fin} and τ_{fin} are the nondimensional oscillation amplitude and period.

2.3 | Fluid Domain (NEPCM)

The working fluid is an NEPCM encapsulated nanoparticles dispersed in a base fluid. To facilitate the numerical solution, assumptions are made while keeping the acceptable physical approximations [5].

- The NEPCM consists of a core (PCM) and a shell.
- The fusion of the PCM occurs at T_f, where $T_f \in \;]T_c; T_h[$.
- Boussinesq approximation for the fluid.
- Steady and incompressible flow.
- A local thermal equilibrium is assumed between the nanoparticles and the base fluid.

The mass properties of a suspension are expressed by:

Let us begin with the density of the mixture, which can be expressed as given below [29]:

$$\rho_b = \phi\rho_p + (1 - \phi)\rho_f. \quad (7)$$

In this equation, ϕ is the concentration of NEPCM particles, ρ refers to the density of the NEPCM nanoparticles, and ρ_f indicates the density of the base fluid.

The PCM particles encapsulated at the nanometer scale, being synthesized in the form of a core and a shell, have their effective density evaluated as follows:

$$\rho_b = \iota\rho_c + (1 + \iota)\rho_c\rho_s/\rho_s. \quad (8)$$

Here, the indices s and c refer to the shell/core, respectively, while l indicates the weight ratio of the core relative to the shell.

The specific heat capacity of a mixture can also be formulated as follows [30]:

$$C_{p_b} = (1 - \phi)\rho_f C_{p_f} + \phi\rho_p C_{p_p}/\rho_b. \quad (9)$$

The total heat capacity of a nanoparticle that is encapsulated can be determined in the following manner:

$$Cp_b = (Cp_{c,l} + \iota Cp_s)\rho_c\rho_s/(\rho_s + \iota\rho_c)\rho_p. \quad (10)$$

The PCM core's specific heat, marked by the index c,l, is determined as the mean of the liquid/solid specific heat capacities [30]:

$$C_{p_c} = C_{p_{c,l}} + \left\{\frac{\pi}{2}\cdot\left(\frac{h_{\text{sf}}}{T_{\text{Mr}}} - C_{p_{c,l}}\right)\cdot\sin\left(\pi\frac{T - T_l}{T_{\text{Mr}}}\right)\right\}$$
$$* \begin{cases} 0, & T^o < T_f^o - T_{\text{Mr}}^o/2, \\ 1, & T_f^o - T_{\text{Mr}}^o/2 < T^o < T_f^o + T_{\text{Mr}}^o/2, \\ 0, & T^o > T_f^o + T_{\text{Mr}}^o/2, \end{cases} \quad (11)$$

The following equation can be used to evaluate the volumetric thermal expansion of the nanoparticle mixture and the base fluid [31]:

$$\beta_b = \phi\beta_p + (1 - \phi)\beta_f. \quad (12)$$

The thermal conductivity and dynamic viscosity of the mixture of the nanoparticle and base fluid can be modeled using the following linear relations [31]:

$$\frac{k_b}{k_f} = 1 + Nc\phi. \quad (13)$$

Here, Nc refers to the thermal conductivity.

$$\frac{\mu_b}{\mu_f} = 1 + Nv\phi, \quad (14)$$

where Nv denotes the dynamic viscosity.

In our study, we consider that Nc and Nv are constants, or we observe that the synthesized nanofluid represents the dependency of the suspension on a variation in the nanoparticle's concentration. These relations are valid only for $\phi < 5\%$.

The core PCM considered in this study undergoes a phase change, necessitating the inclusion of latent heat in the calculation of its specific heat. To account for this, a sinusoidal profile is used to model the latent heat component within the specific heat during the phase transition.

The continuity, momentum (x and y components), and heat conservation equations for the mixture can be formulated as follows:

$$\frac{\partial u}{\partial x} + \frac{\partial u}{\partial y} = 0, \tag{15}$$

$$\left(\frac{\rho_b}{\rho_f}\right)\left(u\frac{\partial u}{\partial x} + v\frac{\partial u}{\partial y}\right) = -\frac{\partial P}{\partial x} + Pr\left(\frac{\mu_b}{\mu_f}\right)\left(\frac{\partial^2 u}{\partial x^2} + \frac{\partial^2 u}{\partial y^2}\right), \tag{16}$$

$$\left(\frac{\rho_b}{\rho_f}\right)\left(u\frac{\partial v}{\partial x} + v\frac{\partial v}{\partial y}\right) = -\frac{\partial P}{\partial x} + Pr\left(\frac{\mu_b}{\mu_f}\right)\left(\frac{\partial^2 v}{\partial x^2} + \frac{\partial^2 v}{\partial y^2}\right) + RaPr\left(\frac{\beta_b}{\beta_f}\right)T, \tag{17}$$

$$Cr\left(u\frac{\partial T}{\partial x} + v\frac{\partial T}{\partial y}\right) = \left(\frac{k_b}{k_f}\right)\left(\frac{\partial^2 T}{\partial x^2} + \frac{\partial^2 T}{\partial y^2}\right), \tag{18}$$

$$Cr = (\rho C_p)_b / (\rho C_p)_f, \tag{19}$$

where Cr denotes the mixture's thermal capacity ratio, which can be explained by [32]

$$Cr = (1 - \phi) + \phi\frac{(C_{p_{c,\iota}} + \iota C_{p_s})\rho_c\rho_s}{C_{p_f}(\rho_s + \iota\rho_c)\rho_f}$$
$$+ \phi\frac{(T_w - T_c)}{T_{Mr}}\left\{\frac{\pi\rho_c\rho_s}{2C_{p_f}(\rho_s + \iota\rho_c)\rho_f}\left(\frac{h_{sf} - C_{p_{c,\iota}}T_{Mr}}{(T_w - T_c)}\right)\right\}f, \tag{20}$$

where f can be expressed as [32]

$$f = \frac{\pi}{2}\cdot\sin\left(\frac{\pi}{\delta}\left(T - T_f + \frac{\delta}{2}\right)\right)*\xi, \tag{21}$$

$$\xi = \begin{cases} 0, & T < -\delta/2 + T_f, \\ 1, & -\delta/2 + T_f < T < +\delta/2 + T_f, \\ 0, & T > +\delta/2 + T_f, \end{cases} \tag{22}$$

and

$$T_f = \frac{T_f^o - T_c^o}{T_w^o - T_c^o} \quad \text{and} \quad \delta = \frac{T_{Mr}}{T_w^o - T_c^o}, \tag{23}$$

where T_f is the dimensionless fusion temperature, k is the ratio of sensible heat capacity, and d is the dimensionless fusion range.

The term $\left(\frac{(\rho_c\rho_s)}{(C_{p_f}(\rho_s + \iota\rho_c)\rho_f)}\right)\left(\frac{(h_{sf} - C_{p_{c,\iota}}T_{Mr})}{(T_w - T_c)}\right)$ accounts for both latent and sensible heat contributions. T_{Mr} indicates the phase change interval temperature, which is assumed to be narrow. The Stefan number is typically introduced as [32]

$$Ste = \frac{(\rho C_p)_f(T_w - T_c)(\rho_s + \iota\rho_c)}{(h_{sf}\rho_s\rho_c)}. \tag{24}$$

Equation (22) can be written as follows:

$$\left((1 - \phi) + \phi\lambda + \frac{\phi}{\delta Ste}f\right)\left(u\frac{\partial T}{\partial x} + v\frac{\partial T}{\partial y}\right) = (1 + Nc\phi)\left(\frac{\partial^2 T}{\partial x^2} + \frac{\partial^2 T}{\partial y^2}\right). \tag{25}$$

2.4 | Boundary Conditions

$T_c = 0$ and $T_h = 1$ on the lateral walls (right and left, the base of the fin at $T_h = 1$, and the upper and lower walls) are assumed to be adiabatic.

Thermal equilibrium between the fluid and the solid is

$$k_s\frac{\partial T}{\partial t} = k_f(1 + Nc\phi)\frac{\partial T}{\partial t}. \tag{26}$$

The corresponding boundary conditions for the fluid–structure coupling are written as follows [15]:

$$\frac{\partial d_{fin}}{\partial t} = u, \quad E\sigma \cdot n = -P + \mu_f(1 + Nv\phi)(\nabla u + (\nabla u)^T), \tag{27}$$

$$P = 0.$$

Ultimately, the key parameter in this investigation is the Nusselt number. The local convective heat transfer rate, represented by the Nusselt number, along the heated boundary is given by [33]

$$Nu = h_y L/k \tag{28}$$

and

$$Nu = -\frac{k_b}{k_f}\frac{\partial T}{\partial x}\bigg|_{x=0}. \tag{29}$$

After mathematical simplification, the following expression represents the average Nusselt number:

$$Nu = -\left(1 + Nc\phi\right)\int_0^1 \frac{\partial T}{\partial x}\bigg|_{x=0}. \tag{30}$$

3 | Numerical Simulation

For solving the problem numerically, The finite element method based on the Galerkin approach to discretize the governing equations of both the solid (fin) and fluid domains, as well as the boundary conditions. A more in-depth analysis of this method is examined in [34, 35]. The coupling between the two phenomena—FSI and NEPCM behavior—is ensured through a monolithic coupling approach. A comparison between this method and the partitioned method is discussed in [36]. In this approach, the governing equations of the phenomena are solved simultaneously using an implicit time-stepping scheme and a first-order upwind spatial discretization. Since the structure moves with a periodic motion, a moving mesh is essential to track the fin's displacement and dynamically adapt the fluid mesh around it [34, 35, 37].

The time integration was carried out using a fully implicit backward differentiation formula (BDF) scheme to ensure stability for transient coupled problems. The linear systems arising from each time step were solved using a direct solver parallel direct sparse solver, with relative tolerance set below 10^{-6} to ensure numerical convergence. The entire numerical procedure was implemented in COMSOL Multiphysics, which allows direct coupling of fluid, thermal, and structural physics. The built-in Moving Mesh (Arbitrary Lagrangian–Eulerian [ALE]) and FSI interfaces were used to handle the domain deformation and the fin's motion.
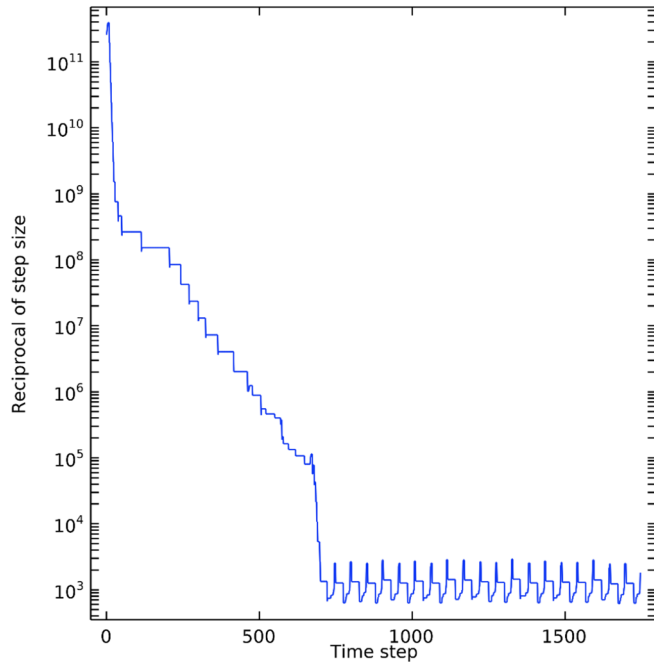
To ensure the convergence of the numerical method, the residuals were monitored at each iteration. Figure 2 shows the evolution of the residuals versus the number of iterations for a representative case, confirming stable convergence below the threshold of 10^{-6}.

3.1 | Mesh Testing and Time Step

In this section of the study, we present the meshing model used. To capture the structural motion, we employed the ALE approach moving mesh method, which combines the advantages of both Eulerian and Lagrangian formulations. Figure 3 provides an overview of the types of meshes used in this study. Compared with partitioned approaches, the monolithic coupling scheme adopted here provides better numerical stability and stronger convergence behavior, especially when dealing with large structural deformations or tight thermal–mechanical interactions.

For the fluid domain, a triangular mesh was applied, as it is ideal for capturing thermal boundary layers and regions with high velocity gradients. For the solid domain, quadrilateral elements were used, as they provide better accuracy in calculating deformations and stresses on the flexible fin.

To ensure the consistency of the numerical results (average Nusselt number) is independent of mesh refinement beyond a certain resolution, a mesh sensitivity test was conducted. Four mesh generations were considered: coarse, intermediate, fine, and very fine. The number of elements associated with each generation is presented in Table 1. The numerical results for these mesh generations are shown in Figure 4, which illustrates the effect of the number of elements on the development of the Nusselt number over dimensionless time at $Ra = 10^5$ and $Ste = 0.313$.

It is noticeable that as the number of elements increases from Case 1 to Case 4, the curves converge. Beyond Cases 3 and 4, an exact match is recorded, indicating that further refinement has
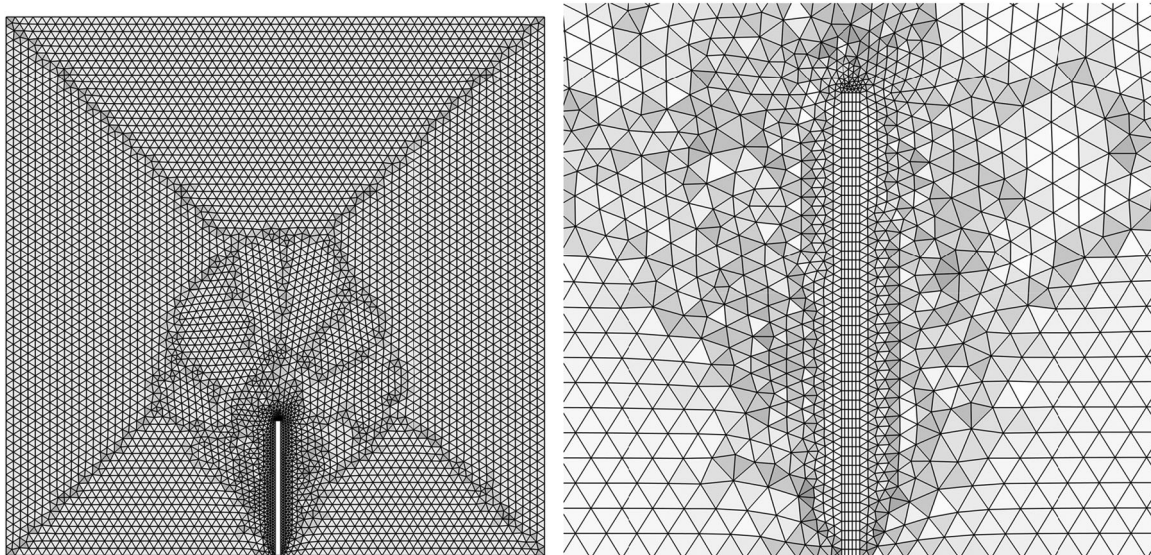

FIGURE 2 | Convergence behavior of the iterative solver showing the residuals as a function of iteration number for the case $Ra = 10^5$ and $Ste = 0.3$. [Color figure can be viewed at wileyonlinelibrary.com]

FIGURE 3 | Mesh structure developed for the model under investigation.

a negligible impact. On the basis of this observation, Case 3 was selected (corresponding to 10,550 domain elements and 353 boundary elements), as improvements beyond this point are insignificant.

3.2 | Validation

Before presenting the results of the numerical model, it is essential to validate it to ensure its accuracy and reliability. The validation process is carried out by contrasting the results obtained with the existing literature findings.

We begin with a numerical validation using the classical benchmark case of De Vahl Davis, which involves a differentially heated square cavity, with the left wall subjected to heating and the right wall to cooling. The validation results are presented in Table 2. The computational findings show an error of less than 1% for Rayleigh numbers $Ra = 10^4$, 10^5, and 10^6, which can be attributed to differences in spatial discretization, time-stepping schemes, or physical assumptions.

A second validation was performed against an experimental investigation carried out by Calcagni et al. [40], where the authors investigated the effect of a heat source with varying length ratios on the Nusselt number. The numerical results, presented in Figure 5, correspond to $Ra = 1.20 \times 10^5$ with a heat source length ratio of 4/5. *The comparison demonstrates a remarkable consistency between the numerical and experimental findings.*

A final validation was conducted using a study by [27], *which analyzed the natural convection and heat transfer in a chamber filled with an NEPCM suspension.* Figure 6 presents a comparison of the dependence of the average Nusselt number of the melting temperature T_f for $Ste = 0.313$ and $Ra = 10^5$, showing very good agreement. Figure 7 further compares isotherms, streamlines, and the heat capacity ratio for a melting temperature of $T_f = 0.3$. The results demonstrate that the streamlines and thermal profiles are in good agreement with those reported in the literature.

TABLE 1 | Sensitivity testing of the mesh involves evaluating different mesh sizes to assess their impact.

	Cases			
	1	**2**	**3**	**4**
Domain elements	3678	5337	10,550	16,004
Boundary elements	239	250	353	415

TABLE 2 | Validation of the Nusselt number results compared with literature results for three Rayleigh numbers of 10^4, 10^5, and 10^6.

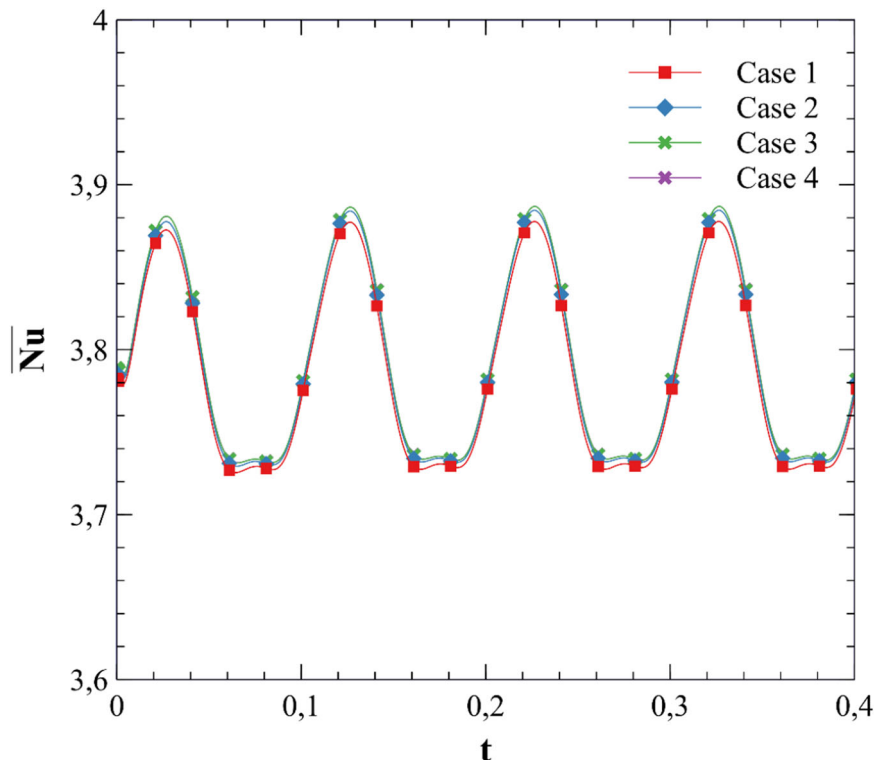|	Ra		
	10^4	**10^5**	**10^6**
De Vahl Davis [38]	2.2430	4.5190	8.8800
Sathiyamoorthy and Chamkha [39]	2.2530	4.5840	8.9210
Present study	2.2452	4.532	8.8250
Error (%)	0.3	0.28	0.6

FIGURE 4 | Grid convergence testing for the Nusselt number on the hot wall across various grid configurations with $Ra = 10^5$, $a_{fin} = \tau_{fin} = 0.1$, and $Ste = 0.313$. [Color figure can be viewed at wileyonlinelibrary.com]
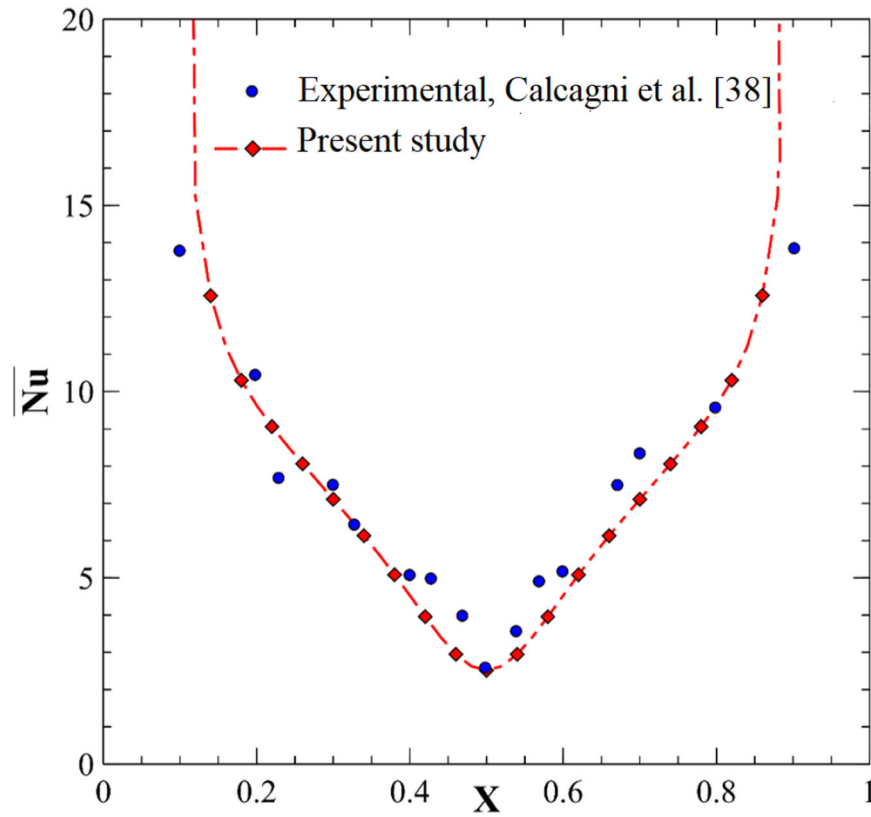
FIGURE 5 | A comparison between the local Nusselt number and the experimental work performed by Calcagni et al. [40] and the current numerical study. [Color figure can be viewed at wileyonlinelibrary.com]

All these comparisons confirm the reliability of the developed numerical model for simulating Natural convection combined with fluid–structure coupling in a fluid containing NEPCMs.

4 | Results and Discussions

In this section, we reach the pivotal aspect of this study, where we present and analyze the results obtained. This study centers on the effects of the fin oscillation, the convection forces characterized by the Rayleigh number Ra (10^4, 10^5, and 10^6), and the Stefan number Ste, which is essential for capturing the phase change behavior. Additionally, we investigate the influence of the fin's periodic motion parameters, namely, the amplitude a_{fin} (0.05, 0.1, and 0.15) and the frequency τ_{fin} (0.1, 0.3, 0.5, and 0.7), on heat exchange by natural convection. The results are analyzed in terms of the average Nusselt number, as well as the distribution of streamlines and isotherms. All other dimensionless parameters are kept constant throughout the study. The solid/fluid thermal conductivity ratio is fixed at $K_s = k_s/k_f = 10$. The thermal conductivity number and the dynamic viscosity number are both set to $Nc = N\nu = 3$. The dimensionless Young's modulus is taken as $E = 10^{11}$, while the fusion temperature is fixed at $T_f = 0.5$. The proportion of volume taken up by NEPCM particles is set to $\phi = 0.05$.

Figures 8 and 9 illustrate the influence of the horizontally oscillating vertical fin and the variation of the Rayleigh number on flow structure and heat transfer, through the analysis of isotherms and streamlines.

In Figure 8, we observe the formation of large primary circulation cells in the core of the cavity. The fluid flow follows a natural convection pattern: it gains energy upon contact with the hot left wall and receives an additional thermal input near the fin. It then moves horizontally along the adiabatic upper wall, where no thermal exchange occurs, before descending along the cold right wall, where it releases its energy. This cycle repeats throughout the simulation. The presence of the flexible fin perturbs the core flow from below, causing a deviation in the fluid trajectory from right to left. Streamlines become denser and more intense near the fin, indicating that the fluid absorbs additional energy when the hot structure oscillates.

As for the isotherms, they appear denser near the left and right walls—where thermal sources are located—as well as at the base and around the heated flexible structure. In the core region of the cavity, the isotherms tend to align horizontally, indicating a more homogeneous thermal mixing of the fluid. In approximately three-quarters of the cavity, the isotherms remain relatively unaffected by the fin oscillation. However, in the lower part of the cavity, the isotherms clearly adapt to the periodic motion of the structure.

The simulations conducted show that the position of the flexible fin significantly affects the thermal behavior of the NEPCM-based fluid. When the fin is placed at the center of the cavity, it interacts more efficiently with the convection cells, which promotes stronger heat exchange. This configuration maximizes the quantity of latent heat absorbed by the NEPCM, resulting in a higher heat capacity ratio (Cr). Conversely, when the fin is located near the lateral walls (right or left), it is less exposed to
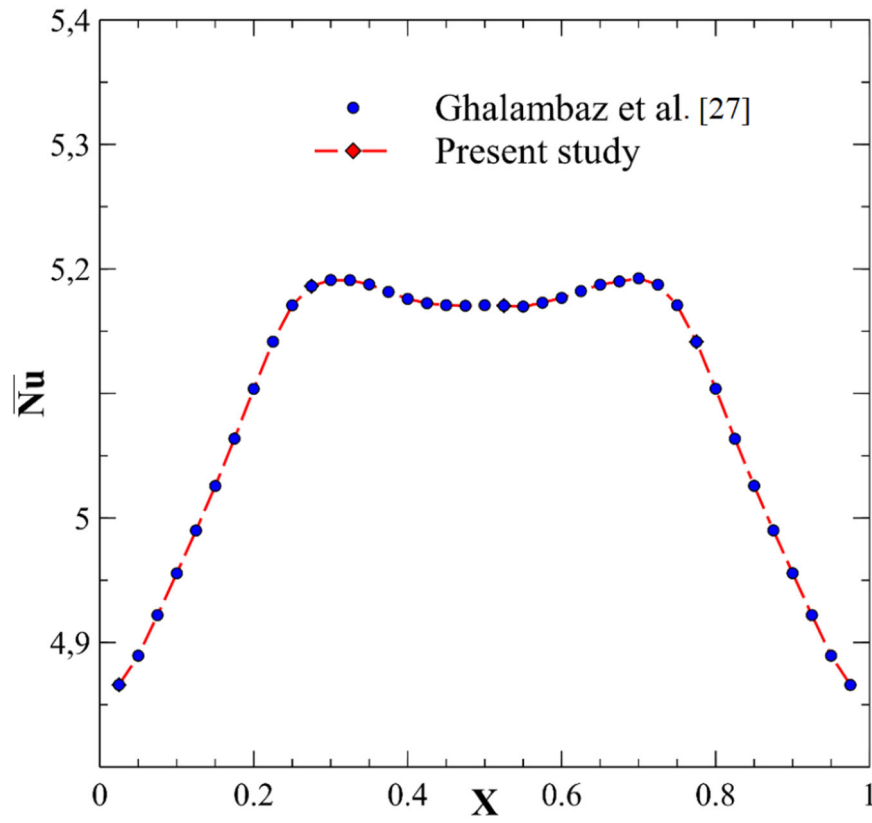
FIGURE 6 | A comparison between the Nusselt number by Ghalambaz et al. [27] and the current numerical study. [Color figure can be viewed at wileyonlinelibrary.com]
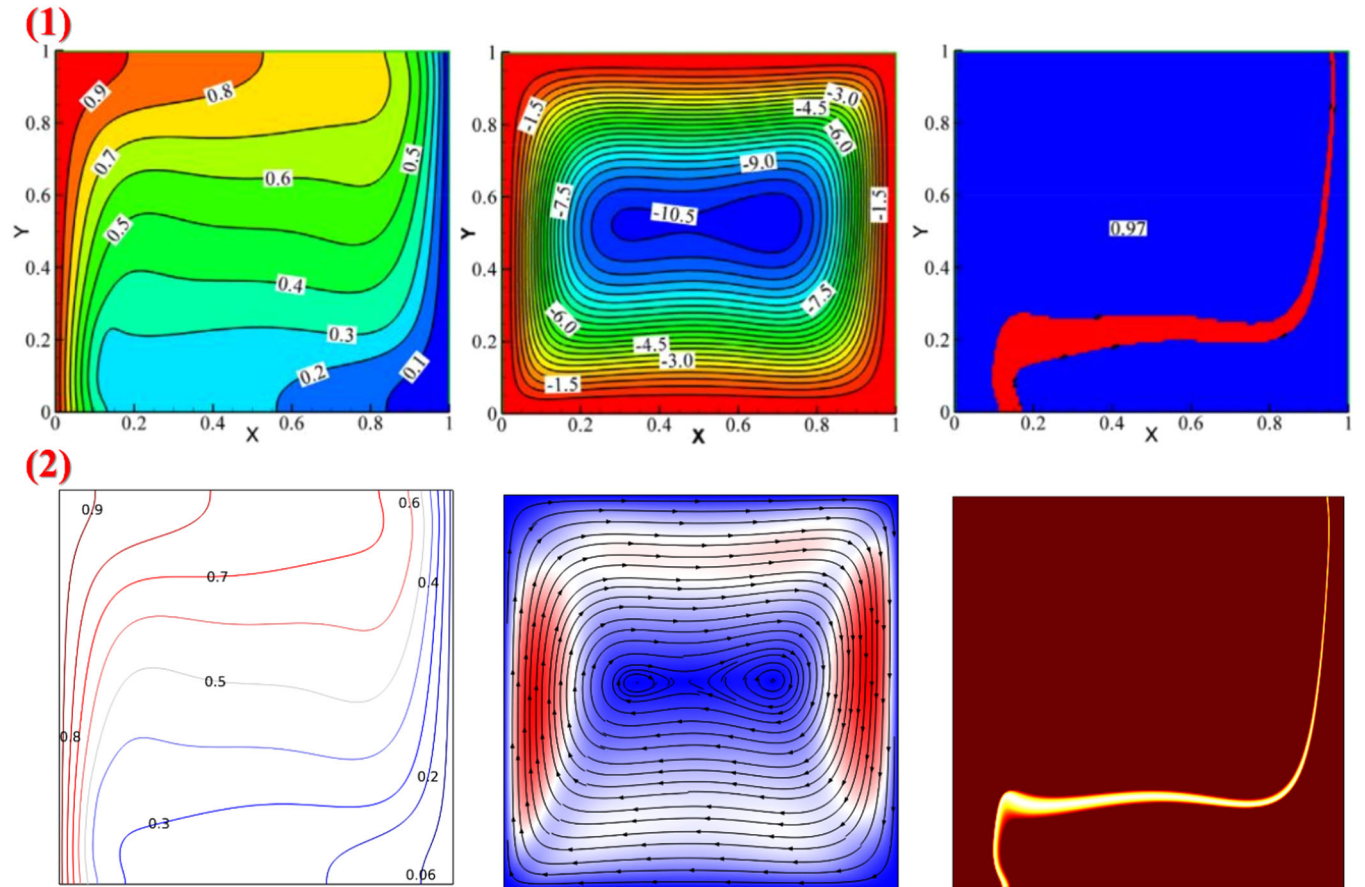

FIGURE 7 | A comparison between isotherms, flow patterns (streamlines), and the ratio of heat capacities for a melting temperature of $T_f = 0.3$, by Ghalambaz et al. [27] and the current numerical study. [Color figure can be viewed at wileyonlinelibrary.com]
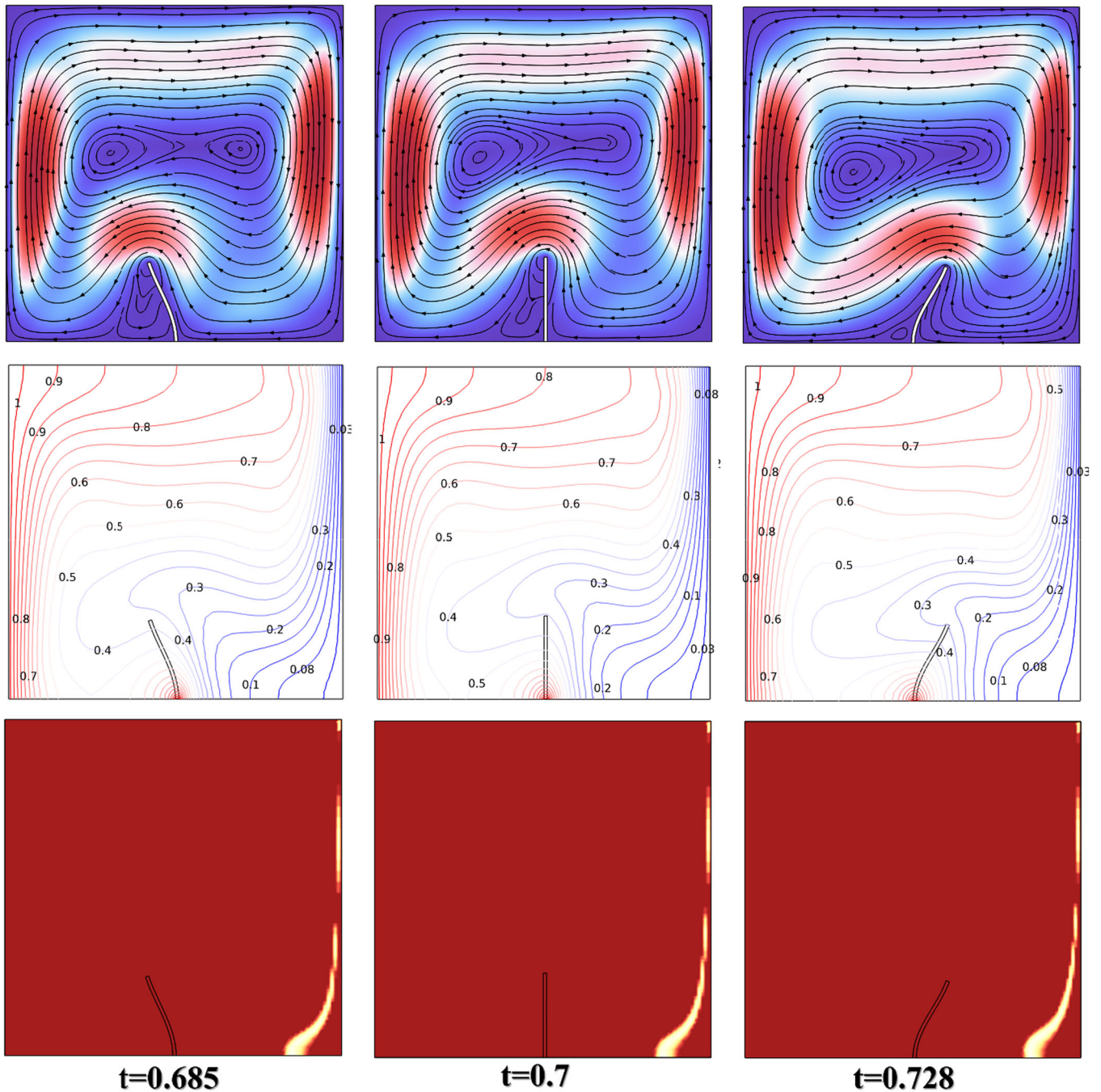
FIGURE 8 | The effect of fin oscillation on the behavior of isotherms, streamlines, and the heat capacity ratio Cr $Ra = 10^5$, $a_{fin} = \tau_{fin} = 0.1$, and $Ste = 0.313$ ($t = 0.685$ left, $t = 0.7$ center, and $t = 0.728$ right). [Color figure can be viewed at wileyonlinelibrary.com]

regions with strong temperature gradients, which limits the thermal activation of the NEPCM and leads to a lower Cr.

In Figure 9, the influence of the Rayleigh number on the distribution of streamlines and isotherms and heat capacity ratio Cr are shown, with fin parameters set to $a_{fin} = \tau_{fin} = 0.1$ and $Ste = 0.313$.

For $Ra = 10^4$, the flow is weak, characterized by a single large primary cell and a secondary one near the fin. The streamlines are sparsely distributed, indicating low fluid velocities and limited interaction with the flexible structure. Upon increasing the Rayleigh number to 10^5 and 10^6, the main circulation

cell becomes more organized and intense. The fluid velocity increases significantly, and secondary vortices appear near the fin. The streamlines become denser throughout the cavity, reflecting stronger convective effects.

Regarding isotherms, for $Ra = 10^4$, they remain nearly vertical and parallel to the sidewalls, indicating that heat transfer is dominated by conduction. In this regime, the presence of the flexible structure and NEPCM particles has a limited impact. However, as Ra increases to 10^5 and 10^6, the isotherms begin to curve horizontally and rise near the heated wall, signaling the onset and intensification of convective transport. A thermal
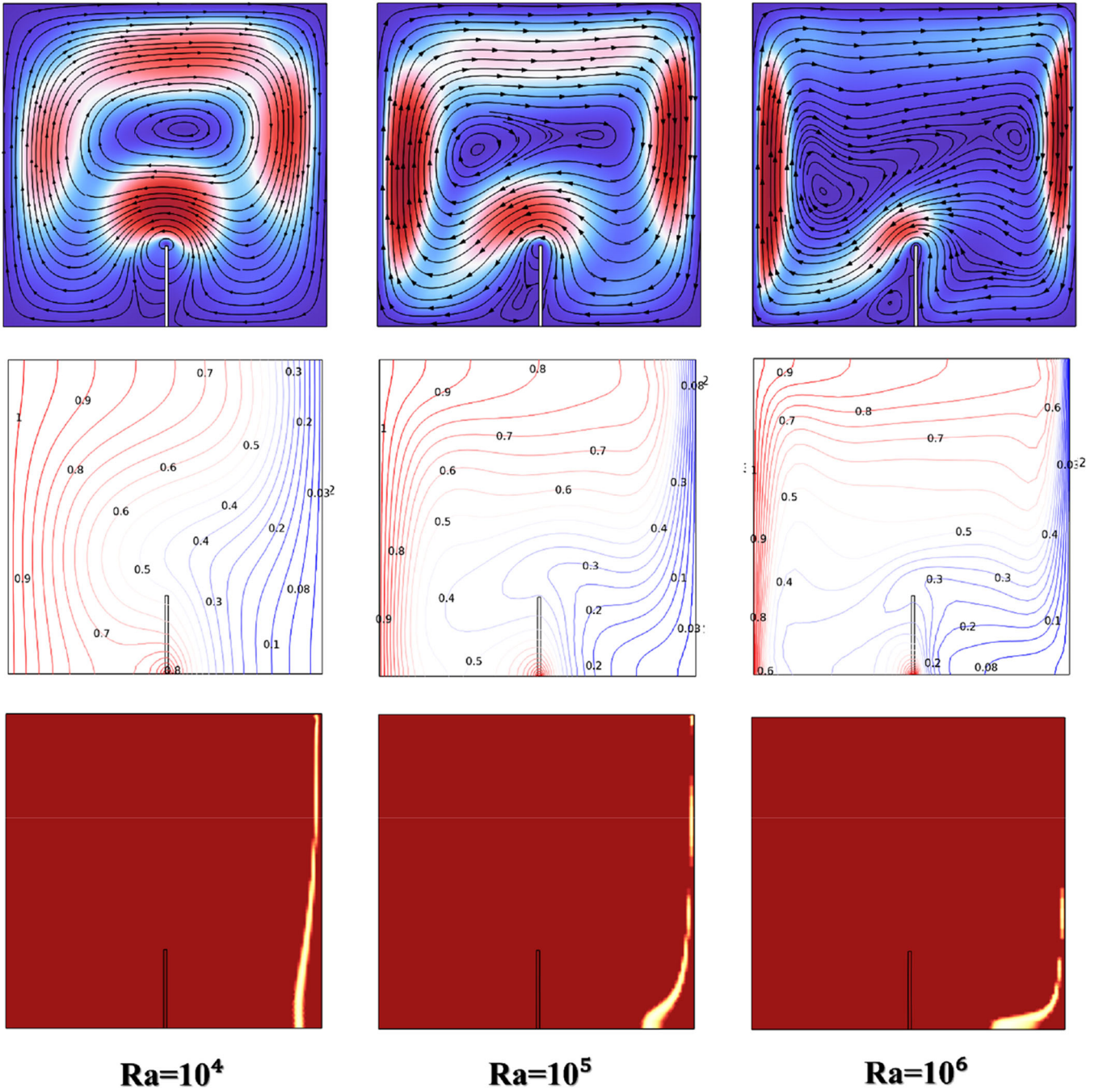
FIGURE 9 | The effect of convection forces ($Ra = 10^4$, 10^5, and 10^6) on the behavior of isotherms, streamlines, and the heat capacity ratio Cr for $a_{\text{fin}} = \tau_{\text{fin}} = 0.1$, $Ste = 0.313$, and $t = 0.7$. [Color figure can be viewed at wileyonlinelibrary.com]

plume develops upward from the hot wall, marking a transition toward convection-dominated behavior.

The periodic motion of the free fin tip becomes increasingly evident with higher Ra, as streamlines adapt to the structural oscillation. The moving fin enhances disturbance in the thermal field, promoting better fluid mixing. In parallel, the NEPCM begins to absorb and redistribute heat more actively, playing the role of a thermal buffer with noticeable effects on the melting zone.

Furthermore, the evolution of Cr with respect to the Rayleigh number (Ra) confirms the importance of natural convection in determining the thermal performance of the system. At low Ra (10^4), heat transfer is dominated by conduction, limiting thermal interactions and resulting in a lower effective heat capacity. As Ra increases (up to 10^6), the strength of the convective rolls becomes more pronounced, enhancing thermal mixing and allowing the NEPCM to absorb and store more energy. Consequently, Cr increases with Ra, indicating that the NEPCM performs more efficiently under strong convective regimes.

Figure 10 illustrates the effect of the Rayleigh number ($Ra = 10^4$, 10^5, and 10^6) on the evolution of the average Nusselt number, for fixed parameters $a_{\text{fin}} = \tau_{\text{fin}} = 0.1$ and $Ste = 0.313$.
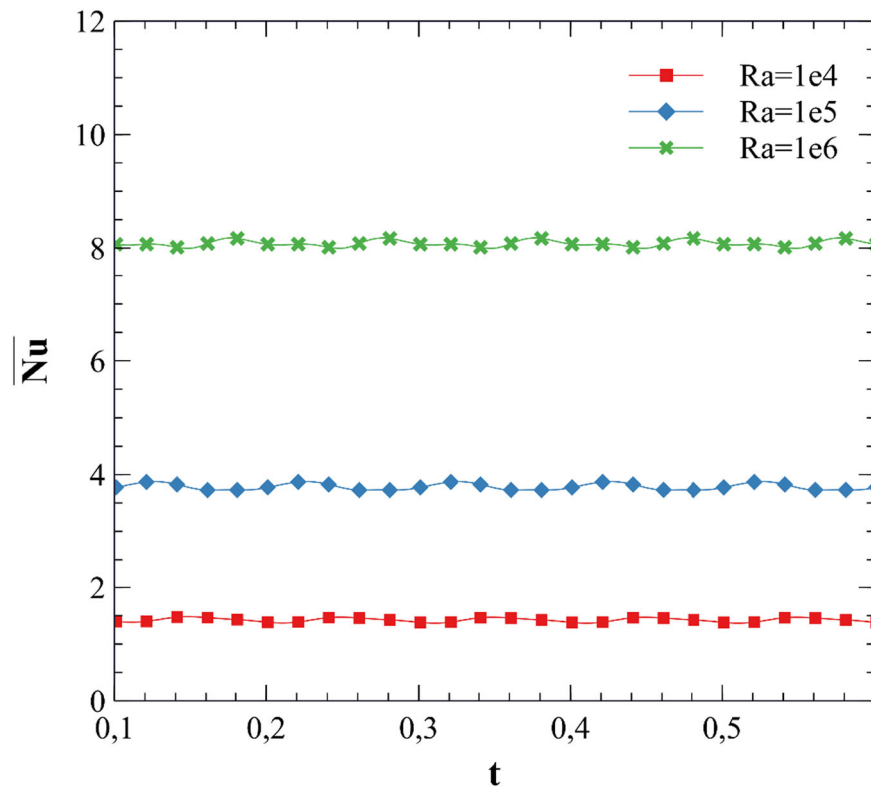
FIGURE 10 | The effect of convection force ($Ra = 10^4$, 10^5, and 10^6) on the average Nusselt number for $a_{\text{fin}} = \tau_{\text{fin}} = 0.1$ and $Ste = 0.313$. [Color figure can be viewed at wileyonlinelibrary.com]

In the low Ra regime ($Ra = 10^4$), the flow regime is nearly conductive. The temperature gradients are weak, resulting in minimal heat transfer rates, with average Nusselt numbers close to 1, typical of pure conduction. As Ra increases to 10^5, the regime transitions to a mixed or transitional state. Thermal gradients along the cavity walls become more pronounced, leading to a significant increase in the Nusselt number, which approaches values around 4. Whereas, for $Ra = 10^6$, the flow becomes strongly convective. Hot fluid is rapidly displaced from the heated left wall and the lower region near the moving fin, enhancing the cooling efficiency along the cold right wall. This leads to steeper thermal gradients and intensified heat transfer. Consequently, the average Nusselt number exceeds 8, reflecting the dominance of convective heat transport in this regime.

Figure 11 illustrates the effect of the Stefan number ($Ste = 0.2$, 0.313, 0.5, and 0.7) concerning the development of the average Nusselt number, for fixed parameters $a_{\text{fin}} = \tau_{\text{fin}} = 0.1$ and $Ra = 10^5$. The numerical results reveal a decreasing trend in the average Nusselt number as the Stefan number increases. This behavior can be explained by the fact that a higher Ste promotes faster melting of the NEPCM, thereby reducing the time during which latent heat significantly contributes to the heat transfer process. Once the NEPCM is fully melted, it behaves as a conventional fluid, and the thermal gradients required to sustain efficient heat exchange diminish. As a result, the system's overall heat transfer capability declines, especially in the presence of a flexible fin, whose dynamic thermal enhancement is weakened as the temperature field becomes more uniform.

The combined analysis of the effects of amplitude (a_{fin}) and period (τ_{fin}) of the periodic motion of the flexible fin highlights their significant influence on heat transfer for fixed parameters $Ste = 0.313$ and $Ra = 10^5$ (see Figures 12 and 13). For small amplitudes ($a_{\text{fin}} = 0.05$) (Figure 12), the disturbance of the velocity field remains limited, which restricts thermal mixing and results in a relatively low average Nusselt number. As the amplitude increases to $a_{\text{fin}} = 0.1$, substantial FSI becomes more pronounced, generating stronger vortical structures and enhancing heat exchange. However, beyond this value ($a_{\text{fin}} = 0.15$), the oscillation may become overly intense, potentially inducing chaotic effects or misaligned recirculation zones that can hinder heat transfer efficiency.

With respect to the oscillation period (Figure 13), a very short time ($\tau_{\text{fin}} = 0.1$) corresponds to a high frequency, causing the fin to move too rapidly for the fluid to respond effectively. This limits thermal penetration and reduces the Nusselt number. Intermediate periods ($\tau_{\text{fin}} = 0.3$ and 0.5) allow for optimal coupling between the fin's motion and the natural fluid dynamics, promoting the formation of organized convective structures and maximizing heat transfer. Conversely, a longer period ($\tau_{\text{fin}} = 0.7$) slows down fluid agitation and reduces the frequency of disturbances, leading to a decline in thermal performance. It can thus be concluded that a moderate amplitude combined with an intermediate period represents the most effective configuration for enhancing the thermal performance of the system under investigation.
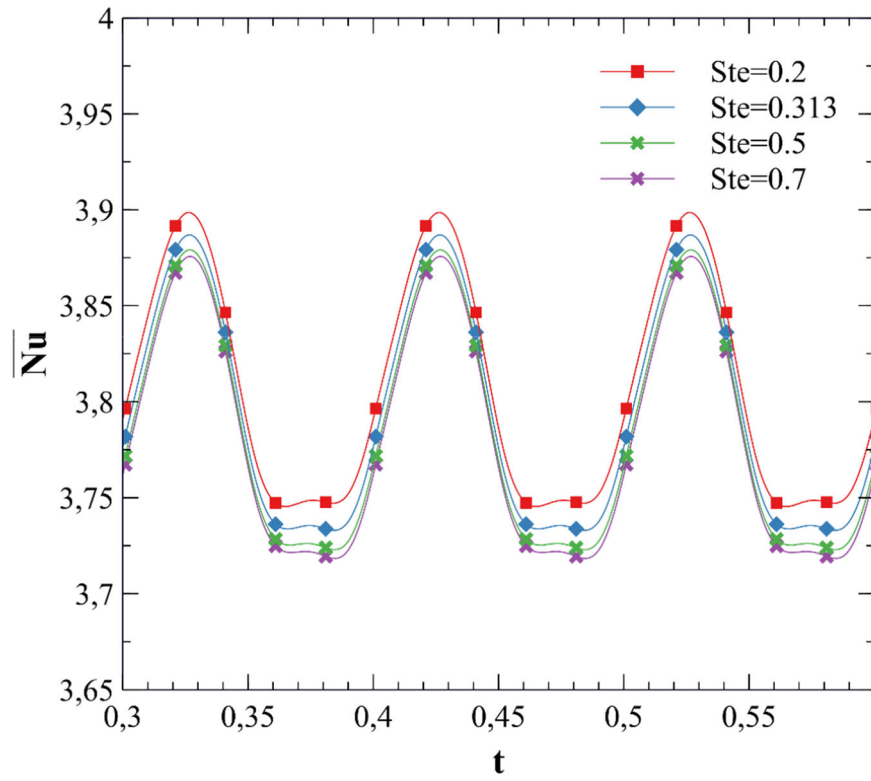
FIGURE 11 | The effect of Stefan number (*Ste*) on the evolution of average Nusselt number for $Ra = 10^5$ and $a_{fin} = \tau_{fin} = 0.1$. [Color figure can be viewed at wileyonlinelibrary.com]

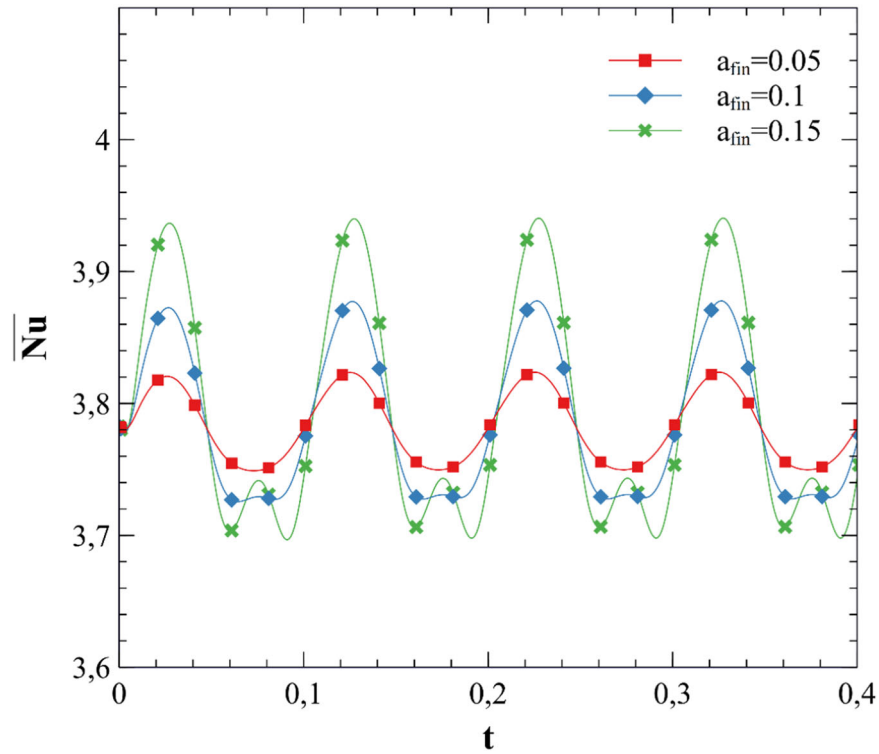

FIGURE 12 | The impact of the fin's amplitude (a_{fin}) concerning the development of the average Nusselt number when $Ra = 10^5$, $\tau_{fin} = 0.1$, and $Ste = 0.313$. [Color figure can be viewed at wileyonlinelibrary.com]
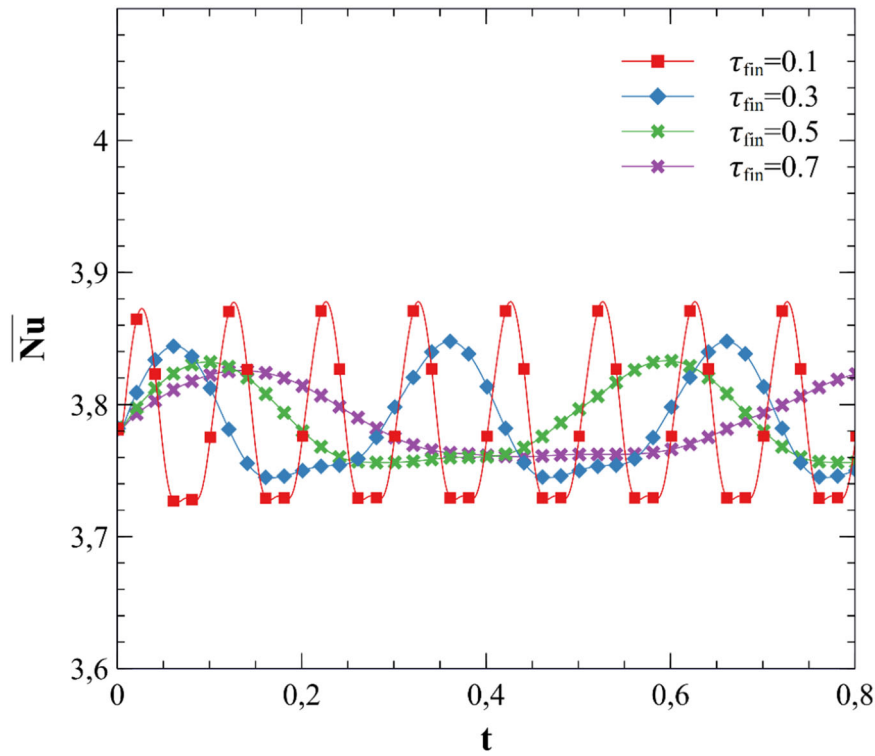
FIGURE 13 | The impact of the fin's frequency (τ_{fin}) concerning the development of the average Nusselt number when $Ra = 10^5$, $a_{\text{fin}} = 0.1$, and $Ste = 0.313$. [Color figure can be viewed at wileyonlinelibrary.com]

5 | Conclusions

The key findings of this numerical investigation into the effect of a sinusoidally oscillating flexible fin in a square cavity filled with NEPCM particles are as follows:

- The periodic motion of the flexible fin introduces significant improvements in the primary natural convection flow. This leads to localized enhancement of heat transfer, especially in the lower part of the cavity.

- Increasing the Rayleigh number from 10^4 to 10^6 transitions the system from a conduction-dominated regime to a convection-dominated one. This results in stronger interactions between the fluid, the NEPCM, and the moving fin, reflected by a marked increase in the average Nusselt number.

- A higher Stefan number accelerates the melting process of the NEPCM particles, reducing their ability to store latent heat. This weakens the thermal effect of the fin and slightly degrades the overall heat transfer performance.

- When the flexible fin is located at the center of the cavity, the interaction with the natural convective flow is maximized, leading to an increase in the heat capacity ratio (Cr), particularly at higher Ra.

- Optimal heat transfer is achieved with a moderate amplitude (e.g., $0.1 \leq a_{\text{fin}} \leq 0.15$) and an intermediate oscillation period (e.g., $\tau_{\text{fin}} = 0.3$–0.5). These conditions provide the best synchronization between structural motion and thermal fluid response.

Future Work

To further develop this study, future studies may extend the model to three-dimensional domains, consider more complex fin geometries, or include various excitations to the flexible fin.

Nomenclature

a, b	length and width of fin (m)
a_{fin}	fin amplitude
C_f	heat capacity per unit of mass (J·kg^{-1}·K^{-1})
Cr	heat capacity ratio
d_s	displacement vector
E	Young's modulus
f	dimensionless phase transition function
F_v	body force vector
g	gravitational acceleration (m·s^{-2})
h	thermal convective coefficient (W·m^{-2}·K^{-1})
k	thermal conductivity (W·m^{-1}·K^{-1})
L	cavity length (m)
Nc	conductivity parameter
Nu	Nusselt number
$N\upsilon$	viscosity parameter
P	dimensionless pressure
Pr	Prandtl number
Ra	Rayleigh number

Ste	Stefan number
t	dimensionless time
T_{Mr}	phase change temperature (K)
u, v	dimensionless velocity components
u°, v°	dimensional velocity components (m·s^{-1})
x_{fin}	horizontal displacement of the fin
x, y and X, Y	dimensional and dimensionless Cartesian co-ordinates (m)

Greek Symbols

α	thermal diffusivity (m^2·s^{-1})
δ	nondimensional parameter of fusion range
ι	core-shell weight ration
λ	ratio of the heat capacity of the NEPCM nanoparticles to the base fluid
μ	dynamic viscosity (kg·m^{-1}·s^{-1})
ν	kinematic viscosity (m^2·s^{-1})
υ	Poisson's ration
ϕ	volume fraction of NEPCM nanoparticles
ρ	density (kg·m^{-3})
σ	stress tensor
τ	period of fin
τ_{fin}	fin period

Subscripts

b	suspension's bulk properties
c	core of NEPCM particles/cold wall
f	fusion property/fluid/base fluid
h	hot
l	liquid cores
P	encapsulated nanoparticles
r	ratio
s	nanoparticles' shell

Conflicts of Interest

The authors declare no conflicts of interest.

Data Availability Statement

The authors have nothing to report.

References

1. A. M. Hassan, M. A. Alomari, H. Q. Birdawod, et al., "Hydrothermal and Entropy Analysis of Micro-Polar NEPCM With Exothermic Reactions and Magnetic Fields," *Energy* 316, no. January (2025): 134479, https://doi.org/10.1016/j.energy.2025.134479.

2. A. M. Hassan, M. A. Alomari, Q. H. Al-Salami, F. Alqurashi, M. A. Flayyih, and A. M. Sadeq, "Numerical Analysis of MHD Combined Convection for Enhanced CPU Cooling in NEPCM-Filled a Trapezoidal Cavity," *International Communications in Heat and Mass Transfer* 159, no. PD (2024): 108343, https://doi.org/10.1016/j.icheatmasstransfer.2024.108343.

3. A. M. Hassan, M. A. Alomari, Q. H. Al-Salami, F. Q. A. Alyousuf, F. Alqurashi, and M. A. Flayyih, "Numerical Analysis of Hydrothermal Performance and Entropy Generation in an Active Cooling System: A Case Study With NEPCM, Double-Diffusive Mixed-Convection and MHD," *Case Studies in Thermal Engineering* 61, no. August (2024): 105064, https://doi.org/10.1016/j.csite.2024.105064.

4. F. L. Rashid, A. K. Hussein, E. H. Malekshah, A. Abderrahmane, K. Guedri, and O. Younis, "Review of Heat Transfer Analysis in Different Cavity Geometries With and Without Nanofluids," *Nanomaterials* 12, no. 14 (2022): 2481, https://doi.org/10.3390/nano12142481.

5. A. Aissa, A. Belazreg, H. Laidoudi, S. Mohammed, O. Younis, and A. Alazzam, "Enhanced Heat Transmission in a Triangular Enclosure With a Rotating Cooled Wall Using Nano-Encapsulated Phase Change Material Nanofluid Under Mixed Convection," *Case Studies in Thermal Engineering* 54, no. October 2023 (2024): 103992, https://doi.org/10.1016/j.csite.2024.103992.

6. A. Abderrahmane, N. A. A. Qasem, A. Belazreg, et al., "Convection Flow of Nano-Encapsulated Phase Change Material in Wavy Chamber With Double Sliding Walls, Flame-Shaped Heating Source, and Magnetic Force," *Case Studies in Thermal Engineering* 56, no. September 2023 (2024): 104250, https://doi.org/10.1016/j.csite.2024.104250.

7. A. Abderrahmane, O. Younis, S. E. Ahmed, A. Mourad, Z. Raizha, and A. Ahmed, "Magnetic Mixed Convection Within Wavy Trapezoidal Thermal Energy Storage Systems Using Nano Enhanced Phase Change Material," *Scientific Reports* 14, no. 1 (2024): 1–14, https://doi.org/10.1038/s41598-024-80802-7.

8. M. Ghalambaz, I. Pop, M. Sheremet, and M. H. Ali, "Numerical and Artificial Neural Network Analysis of Magnetohydrodynamic Natural Convection in a Nano-Encapsulated Phase Change Suspension Filled Quadrantal Circular Enclosure," *Journal of Applied and Computational Mechanics* 11, no. 4 (2025): 929–945, https://doi.org/10.22055/jacm.2024.47986.4891.

9. H. S. S. Aljibori, M. Ghalambaz, A. Akremi, O. Younis, M. Baro, and F. Alresheedi, "Conjugate Entropy Generation and Heat Transfer in a Wavy Walls' Enclosure Containing a Suspension of Dilute Nano-Encapsulated Phase Change Material," *Journal of Taibah University for Science* 19, no. 1 (2025): 2465043, https://doi.org/10.1080/16583655.2025.2465043.

10. S. Hussain, P. Jayavel, B. Almutairi, and K. Ramesh, "Investigation of MHD Oxytactic Microorganisms With NEPCMs in Rectotrapezoidal Enclosure With FEM: Applications to Energy Storage Technologies," *Journal of Magnetism and Magnetic Materials* 592, no. November 2023 (2024): 171808, https://doi.org/10.1016/j.jmmm.2024.171808.

11. S. Hussain, A. M. Aly, N. Alsedias, and A. Batur, "Integrating Artificial Intelligence in Investigating Magneto-Bioconvection Flow of Oxytactic Microorganisms and Nano-Enhanced Phase Change Material in H-Type Cavity," *Thermal Science and Engineering Progress* 49, no. November 2023 (2024): 102497, https://doi.org/10.1016/j.tsep.2024.102497.

12. M. Ghalambaz, E. Jamesahar, M. A. Ismael, and A. J. Chamkha, "International Journal of Thermal Sciences Fluid–Structure Interaction Study of Natural Convection Heat Transfer Over a Flexible Oscillating Fin in a Square Cavity," *International Journal of Thermal Sciences* 111 (2017): 256–273, https://doi.org/10.1016/j.ijthermalsci.2016.09.001.

13. A. I. Alsabery, M. A. Sheremet, M. Ghalambaz, A. J. Chamkha, and I. Hashim, "Fluid–Structure Interaction in Natural Convection Heat Transfer in an Oblique Cavity With a Flexible Oscillating Fin and Partial Heating," *Applied Thermal Engineering* 145, no. June (2018): 80–97, https://doi.org/10.1016/j.applthermaleng.2018.09.039.

14. M. Shahabadi, S. A. M. Mehryan, M. Ghalambaz, and M. Ismael, "Controlling the Natural Convection of a Non-Newtonian Fluid Using a Flexible Fin," *Applied Mathematical Modelling* 92 (2020): 669–686, https://doi.org/10.1016/j.apm.2020.11.029.

15. H. Saleh, K. Naganthran, I. Hashim, M. Ghalambaz, and R. Nazar, "Role of Fluid–Structure Interaction in Free Convection in Square Open Cavity With Double Flexible Oscillating Fins," *Alexandria Engineering Journal* 61, no. 2 (2022): 1217–1234, https://doi.org/10.1016/j.aej.2021.04.073.

16. N. Tarek, B. Elhadj, H. Mohammed, and A. Khadidja, "Numerical Simulation of Fluid–Structure Interaction in Undulated Cavity," *International Information and Engineering Technology Association* 41, no. 5 (2023): 1205–1216, https://doi.org/10.18280/ijht.410511.

17. A. K. N. Tarek, B. Elhadj, G. Mohammad, and H. Mohammed, "Fluid–Structure Interaction Study of an Oscillating Heat Source Effect on the Natural Convection Flow," *Heat Transfer* 53, no. 5 (2024): 2369–2390, https://doi.org/10.1002/htj.23037.

18. A. B. Shahrestani, B. Alshuraiaan, and M. Izadi, "Combined Natural Convection-FSI Inside a Circular Enclosure Divided by a Movable Barrier," *International Communications in Heat and Mass Transfer* 126, no. June (2021): 105426, https://doi.org/10.1016/j.icheatmasstransfer.2021.105426.

19. S. A. M. Mehryan, M. Ghalambaz, R. Kalantar, and A. Hajjar, "Free Convection in a Trapezoidal Enclosure Divided by a Flexible Partition," *International Journal of Heat and Mass Transfer* 149 (2020): 119186, https://doi.org/10.1016/j.ijheatmasstransfer.2019.119186.

20. N. Tarek and M. Ismael, "The Role of Periodic Mixing on Thermal Energy Extraction From an L-Shaped Heater Covered by Porous Layer," *Heat Transfer* 54, no. 3 (2024): 1851–1864, https://doi.org/10.1002/htj.23265.

21. M. S. Faltas and S. El-Sapa, "Rectilinear Oscillations of Two Spherical Particles Embedded in an Unbounded Viscous Fluid," *Microsystem Technologies* 25, no. 1 (2019): 39–49, https://doi.org/10.1007/s00542-018-3928-9.

22. A. Al-Hanaya and S. El-Sapa, "Impact of Permeability and Fluid Parameters in Couple Stress Media on Rotating Eccentric Spheres," *Open Physics* 22, no. 1 (2024): 20240112, https://doi.org/10.1515/phys-2024-0112.

23. M. S. Faltas and S. El-Sapa, "Time-Periodic Electrokinetic Analysis of a Micropolar Fluid Flow Through Hydrophobic Microannulus," *European Physical Journal Plus* 139, no. 7 (2024): 575, https://doi.org/10.1140/epjp/s13360-024-05204-0.

24. N. Acharya, "Effects of the Curved Fins on the Entropy Analysis and Hydrothermal Variations of Buoyancy-Driven MWCNT–Fe_3O_4–H_2O Hybrid Nanofluid Flow Within an Annular Enclosure," *Applied Thermal Engineering* 269 (2025): 126100, https://doi.org/10.1016/j.applthermaleng.2025.126100.

25. N. Acharya, "Framing the Effect of Fitted Curved Fins' Curvature on the Flow Patterns and Entropy Analysis of Buoyancy-Driven Magnetized Hybrid Nanofluidic Transport Within an Annular Enclosure," *Journal of Energy Storage* 100 (2024): 113838, https://doi.org/10.1016/j.est.2024.113638.

26. N. Acharya, "Hydrothermal Scenario of Buoyancy-Driven Magnetized Multi-Walled Carbon Nanotube–Fe_3O_4–Water Hybrid Nanofluid Flow Within a Discretely Heated Circular Chamber Fitted With Fins," *Journal of Magnetism and Magnetic Materials* 589 (2024): 171612, https://doi.org/10.1016/j.jmmm.2023.171612.

27. M. Ghalambaz, A. J. Chamkha, and D. Wen, "International Journal of Heat and Mass Transfer Natural Convective Flow and Heat Transfer of Nano-Encapsulated Phase Change Materials (NEPCMs) in a Cavity," *International Journal of Heat and Mass Transfer* 138 (2019): 738–749, https://doi.org/10.1016/j.ijheatmasstransfer.2019.04.037.

28. E. Jamesahar, M. Sabour, M. Shahabadi, S. A. M. Mehryan, and M. Ghalambaz, "Mixed Convection Heat Transfer by Nanofluids in a Cavity With Two Oscillating Flexible Fins: A Fluid–Structure Interaction Approach," *Applied Mathematical Modelling* 82 (2020): 72–90, https://doi.org/10.1016/j.apm.2019.12.018.

29. L. Chai, R. Shaukat, L. Wang, and H. S. Wang, "A Review on Heat Transfer and Hydrodynamic Characteristics of Nano/Microencapsulated Phase Change Slurry (N/Mpcs) in Mini/Microchannel Heat Sinks," *Applied Thermal Engineering* 135 (2018): 334–349, https://doi.org/10.1016/j.applthermaleng.2018.02.068.

30. S. M. H. Zadeh, S. A. M. Mehryan, M. S. Islam, and M. Ghalambaz, "Irreversibility Analysis of Thermally Driven Flow of a Water-Based Suspension With Dispersed Nano-Sized Capsules of Phase Change Material," *International Journal of Heat and Mass Transfer* 155 (2020): 119796, https://doi.org/10.1016/j.ijheatmasstransfer.2020.119796.

31. S. Hussain, F. Ertam, M. B. B. Hamida, H. F. Oztop, and N. H. Abu-Hamdeh, "Analysis of Bioconvection and Oxytactic Microorganisms in a Porous Cavity With Nano-Enhanced Phase Change Materials and Quadrant Heater: Application of Support Vector Regression Based Model," *Journal of Energy Storage* 63 (2023): 107059, https://doi.org/10.1016/j.est.2023.107059.

32. S. A. M. Mehryan, M. Ismael, and M. Ghalambaz, "Local Thermal Nonequilibrium Conjugate Natural Convection of Nano-Encapsulated Phase Change Particles in a Partially Porous Enclosure," *Mathematical Methods in the Applied Sciences* no. January (2020): 1–18, https://doi.org/10.1002/mma.6338.

33. Z. Raizah and A. M. Aly, "Double-Diffusive Convection of a Rotating Circular Cylinder in a Porous Cavity Suspended by Nano-Encapsulated Phase Change Materials," *Case Studies in Thermal Engineering* 24, no. January (2021): 100864, https://doi.org/10.1016/j.csite.2021.100864.

34. J. Sarrate, A. Huerta, and J. Donea, "Arbitrary Lagrangian–Eulerian Formulation for Fluid–Rigid Body Interaction," *Computer Methods in Applied Mechanics and Engineering* 190, no. 24–25 (2001): 3171–3188, https://doi.org/10.1016/S0045-7825(00)00387-X.

35. A. Joda, Z. Jin, J. Summers, and S. Korossis, "Comparison of a Fixed–Grid and Arbitrary Lagrangian–Eulerian Methods on Modelling Fluid–Structure Interaction of the Aortic Valve," *Proceedings of the Institution of Mechanical Engineers, Part H: Journal of Engineering in Medicine* 233, no. 5 (2019): 544–553, https://doi.org/10.1177/0954411919837568.

36. C. Michler, S. J. Hulshoff, E. H. Van Brummelen, and R. D. Borst, "A Monolithic Approach to Fluid–Structure Interaction," *Computer Methods in Applied Mechanics and Engineering* 193, no. 23–26 (2004): 2087–2104, https://doi.org/10.1016/j.cma.2004.01.024.

37. J. Donea, A. Huerta, J. Ponthot, and A. Rodr, "Chapter 14 Arbitrary Lagrangian-Eulerian Methods," in *Encyclopedia of Computational Mechanics*, ed. E. Stein, R. Borst, and T. J. R. Hughes (2024), https://doi.org/10.1002/0470091355.ecm009.

38. G. De Vahl Davis, "Natural Convection of Air in a Square Cavity: A Bench Mark Numerical Solution," *International Journal for Numerical Methods in Fluids* 3, no. 3 (1983): 249–264, https://doi.org/10.1002/fld.1650030305.

39. M. Sathiyamoorthy and A. J. Chamkha, "Analysis of Natural Convection in a Square Cavity With a Thin Partition for Linearly Heated Side Walls," *International Journal of Numerical Methods for Heat & Fluid Flow* 24, no. 5 (2014): 1057–1072, https://doi.org/10.1108/HFF-02-2012-0050.

40. B. Calcagni, F. Marsili, and M. Paroncini, "Natural Convective Heat Transfer in Square Enclosures Heated From Below," *Applied Thermal Engineering* 25, no. 16 (2005): 2522–2531, https://doi.org/10.1016/j.applthermaleng.2004.11.032.